Impact of Load Variability Modelling on Probabilistic Power System Transient Stability

Siyanda Ncwane and Komla A. Folly
Department of Electrical Engineering, University of Cape Town, Cape Town, South Africa
Email: ncwsiy002@myuct.ac.za; Komla.Folly@uct.ac.za

***Abstract*—Load in a power system is variable due to changes in customer demand. Probability Distribution Functions (PDFs) are commonly used to model power system load variability. The PDFs are generally selected based on their fit to load density. However, PDFs selected based solely on their fit to load density cannot be guaranteed to model the load range. PDFs that model the load range can synthesise maximum and minimum load values. The ability of PDFs to synthesise maximum and minimum load values ensures that the modelled load can be used to develop the power system peak and minimum demand. In this paper, PDFs are selected based on: (1) having a good fit to load density and (2) their ability to synthesise the load range. The results show that PDFs with a good fit to load density and that also model the load range result in power system transient stability results that are similar to those produced when measured load is used.**

***Index Terms*—Load variability modelling, load correlation, load range modelling, probabilistic transient stability**

I. Introduction

Load in a power system varies throughout the day due to changes in customer demand. Load variability impacts both active and reactive power flows, and therefore the reliable operation of power systems. Load variability is commonly modelled using Probability Distribution Functions (PDFs) [1]-[3]. Modelling load variability using PDFs entails identifying the shape of the load density and fitting PDFs to the load density. The quantile functions of the fitted PDFs are used to convert load probabilities in the range [0,1] to synthetic load values. Load probabilities are sampled using methods such as Monte-Carlo Simulation (MCS) [4], quasi-MCS [5], and Latin Hypercube Sampling (LHS) [6].

Load variability was modelled in [1], [7], and [8] using the Gaussian PDF. The limitation of the Gaussian PDF is that it can only model unimodal load density that is not skewed. However, load density may be multimodal and skewed [3], [9]. Load variability was modelled in [2], and [9] using the Kernel Density Estimation (KDE). In [3] and [10], load variability was modelled using the Gaussian Mixture Model (GMM). The use of the KDE and GMM PDFs in [2], [3], [9], and [10] enables the modelling of multimodal load densities that are also skewed. The studies performed in [1]-[3], [7]-[9], and [10] do not evaluate the fit of PDFs to the load density since only a single PDF is used. Studies performed in [11], and [12] evaluate the fit of PDFs to load density, and the impact of load modelling on power system load flows. A study performed in [11] modelled load density using the Gaussian, Beta, Log-normal, Gamma, and GMM PDFs. The chi-square (χ^2) statistic was used in [11] to assess how well PDFs modelled the load. The GMM was found in [11] to have a better fit to load density than the Gaussian, Beta, Log-normal, and Gamma PDFs. In [12], load variability was modelled using the GMM PDF. The impact of the modelled load on a network's voltage levels was assessed in [12] using error analysis by comparing the results to those obtained using measured load. It was found in [12] that the measured and modelled load using the GMM PDF produced similar power system voltage results. In the studies performed in [1]-[3] and [7]-[12], it is not evident whether the PDFs can model the load range or not. The PDFs ability to model the load range ensures that they can synthesise maximum and minimum load values. Maximum and minimum load values are used to develop the power system peak and minimum demand.

The objective of this study is to determine whether in addition to a good fit to load density, the ability of PDFs to model the load range should also be assessed during selection. Load variability in this paper is modelled using seven distribution functions, namely, the Gaussian, Rayleigh, Wakeby, Kappa, GMM, KDE, and Logspline Density Estimation (LDE) PDFs. The results show that PDFs with a good fit and model the load range are best for modelling load variability in a power system.

The rest of the paper is organised as follows: Section II presents methods used to investigate the impact of load variability modelling on power system transient stability, Section III presents load variability modelling results, Section IV presents probabilistic power system transient stability results, and Section V is the conclusion.

II. Modelling

A. Load Modelling

1) Static Load Modelling

When performing power system simulations, the load can be modelled using the polynomial model [13]. The load's active and reactive power is modelled using three components, namely, constant impedance (*Z*), constant current (*I*), and constant power (*P*) [13]. In this study, the

Manuscript received October 26, 2021; revised November 27, 2021; accepted December 13, 2021.
Corresponding author: Siyanda Ncwane (email: NCWSIY002@ myuct.ac.za).

doi: 10.18178/ijeetc.11.5.344-350

power system load is modelled as a constant impedance load using:

$$P = P_o\left[p_1\tilde{V}^2 + p_2\tilde{V} + p_3\right] \quad (1)$$

$$Q = Q_o\left[q_1\tilde{V}^2 + q_2\tilde{V} + q_3\right] \quad (2)$$

where P_o and Q_o are the load's constant active and reactive power, p_1, p_2 and p_3 are the active power coefficients, q_1, q_2 and q_3 are the reactive power coefficients, and $\tilde{V}$ is the load's voltage dependency factor.

2) Load Variability Modelling

Load variability is modelled using seven distribution functions, consisting of the Gaussian, Rayleigh, Wakeby, Kappa, GMM, KDE and LDE PDFs. The Gaussian PDF [7], [14] is given by:

$$f(v) = \frac{1}{\sigma\sqrt{2\pi}}\exp\left(-\frac{(v-\mu)^2}{2\sigma^2}\right) \quad (3)$$

where σ is the standard deviation, μ is the mean, and v is the modelled variable.

The Rayleigh PDF [14] is given by:

$$f(v) = \frac{v-\xi}{\beta^2}\exp\left(\frac{-(v-\xi)^2}{2\beta^2}\right) \quad (4)$$

where the location parameter is ξ, the scale parameter is β, and the modelled variable is v.

The Wakeby PDF [14], [15] is given by:

$$f(v) = \left(\alpha\left[1-F(v)\right]^{\beta-1} + \gamma\left[1-F(v)\right]^{-\delta-1}\right)^{-1} \quad (5)$$

where the first scale parameter is α, the second scale parameter is β, the first shape parameter is γ, the second shape parameter is δ, the location parameter is ξ, and the modelled variable is v.

The Kappa PDF [15] is given by:

$$f(v) = \alpha^{-1}\left[1-\frac{K(v-\xi)}{\alpha}\right]^{\frac{1}{K}-1} \times \left[F(v)\right]^{(1-h)} \quad (6)$$

where the first shape parameter is K, the second shape parameter is h, the scale parameter is α, the location parameter is ξ, and the modelled variable is v.

The GMM PDF used in this investigation uses three Gaussian PDFs to model load variability. The GMM PDF [10], [12] is given by:

$$f(v) = \sum_{i=1}^{N}\omega_i\frac{1}{\sigma_i\sqrt{2\pi}}\exp\left[-\frac{(v-\mu_i)^2}{2\sigma_i^2}\right] \quad (7)$$

where the i^{th} Gaussian PDF's weight, standard deviation and mean are given by ω_i, σ_i, and μ_i, respectively, and the modelled variable is v.

The KDE PDF used in this investigation uses Gaussian kernels to model load variability. The KDE PDF [16] is given by:

$$f(v) = \frac{1}{nh}\sum_{i=1}^{n}K\left(\frac{v-v_i}{h}\right) \quad (8)$$

where the Gaussian kernel is K, the number of load samples is n, the kernel bandwidth is h, and the modelled variable is v.

The LDE PDF used in this investigation uses basis-splines (B-splines), which are piecewise polynomials with continuity constraints to model load variability [17], [18]. The LDE PDF [17], [18] is given by:

$$f(v) = \exp\left[\sum_{n=1}^{N}\theta_n B_n(v) - C(\theta)\right] \quad (9)$$

where the B-splines are $B_n(v)$, the coefficients of B-splines is θ_n, the normalising constant is $C(\theta)$, and the modelled variable is v.

3) Load Spatial Correlation

Load in a power system is spatially correlated due to customer demand patterns. The Kendall's tau correlation coefficient is used in this investigation to assess whether the variable load modelled using the PDFs maintains the measured load's spatial correlation. The Kendall's tau correlation coefficient [19], [20] of two variables X and Y is given by:

$$\tau = \frac{2}{n(n-1)}\sum_{i=1}^{n}\sum_{i<j}\text{sgn}\left[(x_i - x_j)(y_i - y_j)\right] \quad (10)$$

where n is the sample size, sgn is the sign function, x_i and x_j are observations from X and y_i and y_j are observations from Y.

4) Load Range

Load probabilities in the range [0,1] are sampled using LHS [6]. Synthetic load values are produced using the fitted PDFs quantile functions from the sampled load probabilities. Measured and synthesised maximum and minimum load values are compared to assess the PDF's ability to model the load range.

B. Probabilistic Power System Transient Stability

The power system's transient stability is investigated using the probabilistic method. Different power system loading conditions are modelled using sampled load data. Time-domain analysis is then used to investigate the power system transient stability by applying three-phase faults on a line. The applied faults are isolated by tripping the line using a fault clearing time of 100 ms.

C. Goodness-of-Fit

The Root Mean Square Error (RMSE) and Mean Absolute Error (MAE) are used to assess the error between modelled and measured load, and the error between the power system's transient stability results produced using measured and modelled load. The RMSE and MAE [15], [21] are given by:

$$\text{RMSE} = \sqrt{\frac{1}{N}\sum_{i=1}^{N}\left(\hat{F}_i - F_i\right)^2} \quad (11)$$

$$\text{MAE} = \frac{1}{N}\sum_{i=1}^{N}\left|\hat{F}_i - F_i\right| \quad (12)$$

where $\hat{F}_i$ and F_i are probabilities of the i^{th} independent and dependent variables, and N is the number of samples.

III. Power System Load Variability Modelling

A. Case Study

The IEEE 9-bus test system shown in Fig. 1 is used as a case study. The test system has three synchronous generators (SGs). The SGs operate in voltage control mode, and each has an IEEET1 excitation system and a BPA_GG governor system. Gen 1 is the reference machine. The active power generated by Gen 3 is set to 85 MW. The active power generated by Gen 2 is set to 0 MW, and the machine is operated as a synchronous condenser.

The IEEE 9-bus test system load is located at buses 5, 6 and 8. Load variability is modelled using residential substation load, measured in 5-minute intervals between January and December 2019. The measured load is normalised using the peak load demand at each load bus. The maximum and minimum load values at the three load buses are shown in Table I.

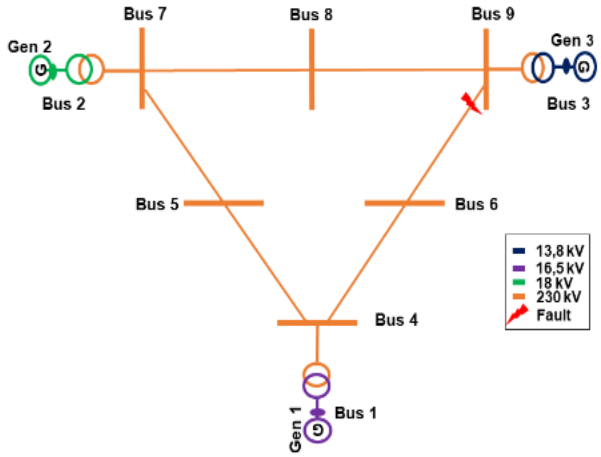

Fig. 1. IEEE 9-bus test system diagram [22].

TABLE I: LOAD RANGE

Load range	Bus 5 Load (MW)	Bus 6 Load (MW)	Bus 8 Load (MW)
Maximum	125.000	90.000	100.000
Minimum	31.604	27.640	14.366

TABLE II: MISSING SUBSTATION LOAD DATA

Loads	Percentage
Bus 5 Load	0.04384%
Bus 6 Load	0.07052%
Bus 8 Load	0.00477%

Table II shows the pre-processed measured load data. Pre-processing the load data shows that there are missing load measurements. The measured load assigned to bus 5 has 0.04384% missing measurements, while the load assigned to bus 6 has 0.07052% missing measurements. On the other hand, the load assigned to bus 8 has 0.00477% missing measurements.

A. Load Variability Modelling

1) Fitting Probability Distribution Functions

The distribution functions are fitted to the load density using tools available in the R-programming language version 3.6.1. Tables III to VII show the parameters of the Gaussian, Rayleigh, Wakeby, Kappa and GMM PDFs used to model load variability.

TABLE III: GAUSSIAN DISTRIBUTION FUNCTION PARAMETERS

Loads	Mean	Standard Deviation
Bus 5 Load	65.204	17.246
Bus 6 Load	57.091	10.617
Bus 8 Load	40.247	15.142

TABLE IV: RAYLEIGH DISTRIBUTION FUNCTION PARAMETERS

Loads	Location	Scale
Bus 5 Load	31.983	26.506
Bus 6 Load	36.640	16.317
Bus 8 Load	11.079	23.273

TABLE V: WAKEBY DISTRIBUTION FUNCTION PARAMETERS

Loads	Location	Scale 1	Scale 2	Shape 1	Shape 2
Bus 5 Load	35.731	62.955	1.268	0.664	0.613
Bus 6 Load	34.966	73.354	5.394	14.914	-0.400
Bus 8 Load	9.044	462.876	32.365	19.568	-0.129

TABLE VI: KAPPA DISTRIBUTION FUNCTION PARAMETERS

Loads	Location	Scale	Shape 1	Shape 2
Bus 5 Load	51.782	27.165	0.499	0.505
Bus 6 Load	52.773	11.587	0.341	0.098
Bus 8 Load	30.877	13.190	-0.017	0.244

TABLE VII: GMM DISTRIBUTION FUNCTION PARAMETERS

Loads	Weight 1	Weight 2	Weight 3	Mean 1	Mean 2	Mean 3	Standard Deviation 1	Standard Deviation 2	Standard Deviation 3
Bus 5 Load	0.249	0.678	0.073	44.544	70.002	91.089	5.303	12.202	12.993
Bus 6 Load	0.336	0.441	0.223	46.095	58.896	70.053	6.004	5.056	5.800
Bus 8 Load	0.091	0.571	0.338	20.480	33.864	56.386	1.336	6.240	15.621

Fig. 2 shows density plots of the measured load modelled using PDFs. The load density at bus 5 is multimodal since it has multiple peaks. The multimodal load density is not modelled by the Gaussian, Rayleigh, Wakeby and Kappa PDFs because they are unimodal. However, the multimodal load density is modelled by the GMM, KDE and LDE PDFs. The GMM PDF models the multimodal load density because it fits three Gaussian PDFs. Also, the multimodal load density is modelled by the KDE and LDE PDFs because they are both non-parametric distribution functions that fit Gaussian kernels and B-splines, respectively, to the load. At buses 6 and 8, load density has a single peak, hence it is unimodal, and all the distribution functions assessed model the load density.

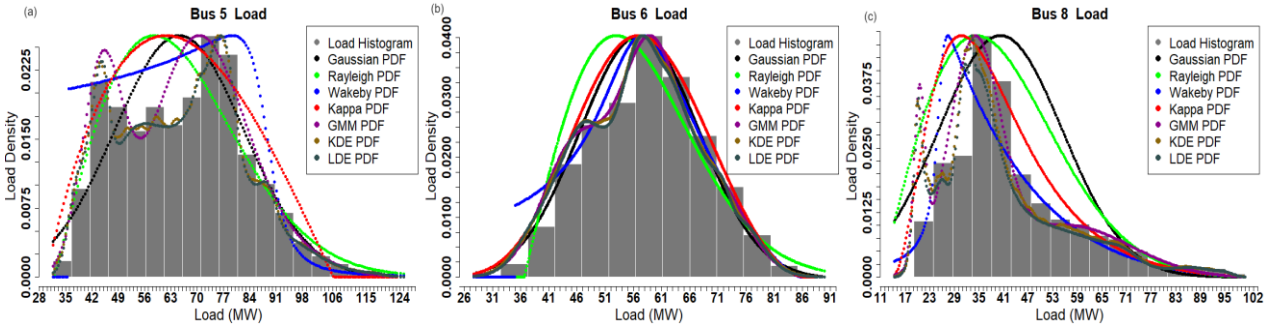

Fig. 2. Load density modelled using PDFs: (a) bus 5 load, (b) bus 6 load, (c) bus 8 load.

TABLE VIII: LOAD SPATIAL CORRELATION

Load	Buses 5 and 6 Load	Buses 5 and 8 Load	Buses 6 and 8 Load
Measured Load	0.418950	0.499111	0.317247
Gaussian Load	0.418930	0.499083	0.317221
Rayleigh Load	0.418930	0.499083	0.317221
Wakeby Load	0.418946	0.499101	0.317241
Kappa Load	0.418944	0.499101	0.317239
GMM Load	0.418930	0.499083	0.317221
KDE Load	0.418950	0.499111	0.317247
LDE Load	0.418930	0.499083	0.317221

The Kendall's tau correlation coefficients of the measured and modelled loads at the three load buses are shown in Table VIII. The spatial correlation of the measured and modelled load at the three load buses is assessed to determine if the modelled load maintains the measured load's spatial correlation. The load Kendall's tau correlation coefficients show that the modelled load preserves the measured load's spatial correlation. Also, the loads Kendall's tau correlation coefficients show that buses 5 and 8 loads have the highest spatial correlation, followed by buses 5 and 6 loads, and lastly, buses 6 and 8 loads.

2) Distribution Function Goodness-of-Fit

The plots of the measured load Empirical Cumulative Distribution Functions (ECDFs) and the fitted PDFs Cumulative Distribution Functions (CDFs) are shown in Fig. 3. It can be seen that the CDFs of the fitted PDFs are closer to the measured bus load ECDFs at higher loads than lower loads. This indicates that the fitted PDFs are more accurate at modelling higher load values than lower load values. The RMSE and MAE results of the fitted distribution functions are shown in Tables IX and X, respectively. The CDFs with the lowest RMSE and MAE are the KDE CDF, followed by the LDE CDF and the GMM CDF. These results indicate that the KDE PDF, followed by the LDE PDF, and then the GMM PDF have a good fit to load density at the three load buses.

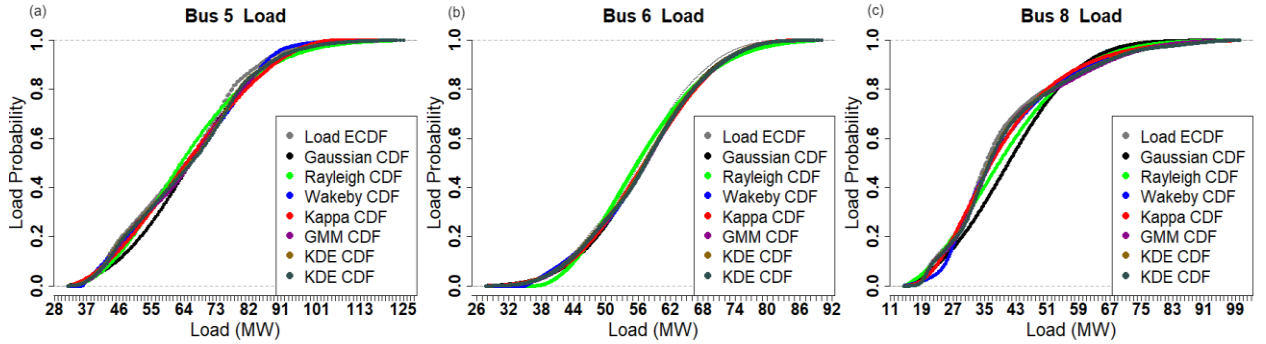

Fig. 3. Load ECDFs modelled using CDFs: (a) bus 5 load, (b) bus 6 load, (c) bus 8 load.

TABLE IX: LOAD MODELLING RMSE RESULTS

Loads	Gaussian CDF	Rayleigh CDF	Wakeby CDF	Kappa CDF	GMM CDF	KDE CDF	LDE CDF
Bus 5 Load	0.02746	0.03403	0.01417	0.02019	0.00907	0.00141	0.00473
Bus 6 Load	0.00997	0.03167	0.00580	0.00850	0.00286	0.00228	0.00234
Bus 8 Load	0.07020	0.04329	0.02465	0.02237	0.00621	0.00117	0.00413

TABLE X: LOAD MODELLING MAE RESULTS

Loads	Gaussian CDF	Rayleigh CDF	Wakeby CDF	Kappa CDF	GMM CDF	KDE CDF	LDE CDF
Bus 5 Load	0.02190	0.02880	0.01093	0.01742	0.00750	0.00118	0.00429
Bus 6 Load	0.00740	0.02644	0.00438	0.00710	0.00228	0.00201	0.00216
Bus 8 Load	0.05541	0.03448	0.02013	0.01912	0.00530	0.00091	0.00347

3) Load Range Synthesis

Table XI shows the synthesised maximum and minimum load using quantile functions of the fitted PDFs. A comparison of Tables I and XI shows that only the KDE and LDE PDFs model the load range at the three load buses. The Gaussian PDF synthesises maximum and minimum load at bus 6. At buses 5 and 8, the Gaussian PDF synthesises maximum load only. Furthermore, at buses 5 and 8, the Gaussian PDF synthesises negative load values, while the minimum load should be positive,

as shown in Table I. The Rayleigh PDF synthesises maximum and minimum load at bus 8. At buses 5 and 6, the Rayleigh PDF synthesises maximum load only. The Wakeby PDF synthesises maximum and minimum load at bus 8. At bus 5, the Wakeby PDF synthesises maximum load only. At bus 6, the Wakeby PDF does not synthesise both maximum and minimum load. The Kappa PDF synthesises maximum and minimum load at bus 8. At buses 5 and 6, the Kappa PDF synthesises minimum load only. The GMM PDF synthesises bus 5 and 6 maximum and minimum load. At bus 8, the GMM PDF synthesises maximum load only, whereas the synthesised minimum load value is negative. This does not agree with the minimum load value shown in Table I, which is positive. The inability of the PDFs to synthesise maximum and minimum load indicates that their upper and lower tails do not extend beyond the measured maximum and minimum load values.

TABLE XI: SYNTHESISED MAXIMUM AND MINIMUM LOAD

Loads	Statistic	Gaussian PDF	Rayleigh PDF	Wakeby PDF	Kappa PDF	GMM PDF	KDE PDF	LDE PDF
Bus 5 Load	**Maximum (MW)**	143.923	166.605	3020.107	106.125	142.809	125.025	128.183
	Minimum (MW)	-12.733	32.049	35.732	29.746	15.864	31.574	24.554
Bus 6 Load	**Maximum (MW)**	105.380	119.268	85.620	86.299	94.543	90.029	95.132
	Minimum (MW)	7.201	36.667	34.966	19.181	19.252	27.606	17.470
Bus 8 Load	**Maximum (MW)**	107.803	127.030	144.367	212.721	122.354	100.030	101.794
	Minimum (MW)	-26.757	11.151	9.047	13.147	-8.984	14.327	12.749

4) Comparison of Distribution Functions

Table XII shows the distribution function with the best fit to load density at the three load buses based on the RMSE and MAE. Also, Table XIII shows distribution functions that can model the load range at the three load buses. Based on fit to load density and their ability to model the load range, the load at the three load buses should be modelled using the KDE PDF. The KDE PDF best fits load density, and models maximum and minimum load at all three load buses among the distribution functions assessed. The LDE PDF has the second-best fit to load density and also models maximum and minimum load at the three load buses.

TABLE XII: DISTRIBUTION FUNCTION WITH HIGH GOODNESS-OF-FIT

Loads	Distribution Function
Bus 5 Load	KDE PDF
Bus 6 Load	KDE PDF
Bus 8 Load	KDE PDF

TABLE XIII: DISTRIBUTION FUNCTION THAT MODELS THE LOAD RANGE

Loads	Distribution Function
Bus 5 Load	KDE, LDE and GMM PDFs
Bus 6 Load	KDE, LDE, GMM and Gaussian PDFs
Bus 8 Load	KDE, LDE, Rayleigh, Wakeby and Kappa PDFs

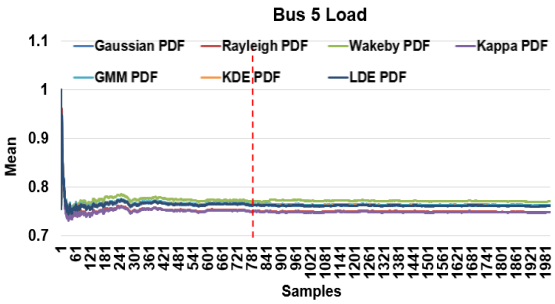

Fig. 4. Bus 5 normalised load moving mean.

IV. POWER SYSTEM TRANSIENT STABILITY ANALYSIS

A. Sample Size

The impact of the modelled load on power system transient stability is assessed using probabilistic transient stability analysis. Load values are randomly sampled from the variable load using MCS. Fig. 4 shows bus 5 normalised load moving mean. The normalised load moving mean figures for buses 6 and 8 are not shown due to the limited space. The normalised load moving mean is used to determine the sample size based on the number of samples required for the load's normalised moving mean to stabilise.

The required number of samples for bus 5 and bus 8 normalised load moving mean to stabilise is about 781. Furthermore, about 541 samples are required for bus 6 normalised load moving mean to stabilise. This indicates that at each load bus, at least about 781 load samples should be used. As a result, in this study, 1000 load samples are used to investigate if the measured and modelled variable load results in similar transient stability of the IEEE 9-bus test system.

B. Probabilistic Power System Transient Stability

For each of the 1000 load samples taken, the transient stability of the IEEE 9-bus test system is assessed using time-domain analysis in Digsilent PowerFactory 2020. The studies are automated using a script developed using Python 3.6 that interfaces to Digsilent PowerFactory using its Application Programming Interface (API). The IEEE 9-bus test system transient stability is assessed by applying three-phase faults on line 6-9, as shown in Fig. 1. The faults are applied on line 6-9, close to bus 9. During the studies, Gen 3's rotor angle deviations are monitored. The applied fault is isolated by tripping the line using a fault clearing time of 100 ms. Applying the fault causes Gen 3's rotor to accelerate due to the generator storing the power it cannot transfer into the power system as kinetic energy. This causes Gen 3's rotor to accelerate, resulting in the rotor angle deviating from its pre-fault value.

Fig. 5 shows ECDFs of Gen 3's rotor angle deviations. Among the PDFs used to model load variability, the load modelled using the KDE and LDE PDFs result in Gen 3's rotor angle deviation ECDFs that closely follow those produced when measured load is used. The ECDFs of Gen 3's rotor angle deviations produced when load variability is modelled using the Gaussian, Rayleigh, Wakeby, Kappa and GMM PDFs do not closely follow those produced when measured load is used. The load modelled using the Gaussian, and GMM PDFs results in Gen 3 rotor angle deviations that are lower than those

produced when measured load is used. This indicates that the load modelled using the two PDFs causes the power system to operate further away from transient instability than when measured load is used. On the other hand, load modelled using the Rayleigh, Wakeby and Kappa PDFs results in Gen 3 rotor angle deviations that are higher than those produced when measured load is used. This indicates that the load modelled using the three PDFs causes the power system to operate closer to transient instability than when measured load is used.

Table XIV shows the range of Gen 3 rotor angle deviations produced when measured and modelled load is used. The range of Gen 3 rotor angle deviations indicates that the generator remains synchronised during the 1000 power system loading conditions assessed. This indicates that when measured and modelled load is used, Gen 3 remains transiently stable. The benefit of considering the impact of load variability on probabilistic power system transient stability is that it makes it possible to identify loading conditions that result in instability and loading conditions that do not. Network loading conditions that result in transient instability can be further investigated to determine why instability occurs.

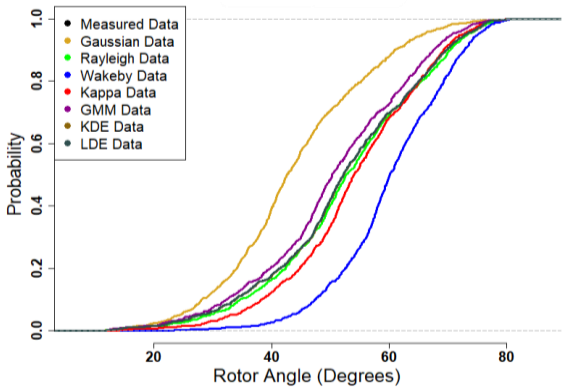

Fig. 5. Gen 3 rotor angle deviation ECDFs when three-phase faults are applied close to bus 9 online 6-9.

TABLE XIV: GEN 3'S ROTOR ANGLE DEVIATION RANGE

Fault location	Measured Data	Gaussian PDF Data	Rayleigh PDF Data	Wakeby PDF Data	Kappa PDF Data	GMM PDF Data	KDE PDF Data	LDE PDF Data
Line 6-9 fault	11.9^0 to 80.6	17.1^0 to 92.2^0	10.9^0 to 80.0^0	-15.1^0 to 80.4^0	4.3^0 to 82.1^0	12.7^0 to 82.8^0	11.8^0 to 80.6^0	11.7^0 to 80.5^0

TABLE XV: GEN 3 ROTOR ANGLE DEVIATION ECDFS RMSE AND MAE RESULTS

Fault location	Gaussian PDF Data	Rayleigh PDF Data	Wakeby PDF Data	Kappa PDF Data	GMM PDF Data	KDE PDF Data	LDE PDF Data
RMSE	0.024701	0.021240	0.013894	0.012772	0.007134	0.001094	0.001182
MAE	0.019452	0.016406	0.010640	0.009718	0.004534	0.000646	0.000742

C. Similarity Analysis of Transient Stability Results

The RMSE and MAE result shown in Table XV compare Gen 3's rotor angle deviation ECDFs obtained when measured and modelled variable load is used. The results indicate that modelling load variability using the KDE PDF produces Gen 3 rotor angle deviations with the lowest RMSE and MAE among the PDFs assessed. Modelling load variability using the LDE PDF produces Gen 3 rotor angle deviations with the second-lowest RMSE and MAE. Furthermore, load modelled using the GMM PDFs produces Gen 3 rotor angle deviations with the third-lowest RMSE and MAE. In Section III, it was found that among the PDFs assessed, both maximum and minimum load was synthesised at the three load buses by the KDE and LDE PDFs. As a result, the KDE PDF is best suitable for modelling load variability at the three load buses, followed by the LDE PDF. The two PDFs are suitable for modelling load variability because they have a good fit to load density at the three load buses, secondly, they model the load range at the three load buses and lastly, the variable load they model produces Gen 3 rotor angle deviation results that are similar to those produced when measured load is used.

V. CONCLUSION

The impact of load variability modelling on power system transient stability was investigated in this paper. Load variability was modelled using the Gaussian, Rayleigh, Wakeby, Kappa, GMM, KDE, and LDE PDFs. It was found that the KDE PDF, followed by the LDE PDF, are suitable for modelling load variability. The two PDFs have a good fit to load density, and they synthesise the load range. Furthermore, it was found that load modelled using the KDE and LDE PDFs produced rotor angle deviations similar to those produced when measured load was used. The study's findings indicate that when modelling power system load variability, in addition to selecting PDFs based on their fit to load density, they should also be selected based on whether they model the load range or not.

CONFLICT OF INTEREST

The authors declare no conflict of interest.

AUTHOR CONTRIBUTIONS

Siyanda Ncwane conceptualised the research, performed the analysis and wrote the paper. Komla A. Folly supervised the research, acquired the research funding, reviewed, and edited the paper. All the authors have approved the final version.

REFERENCES

[1] B. Marah and A. O. Ekwue, "Probabilistic load flows," in *Proc. 50th International Universities Power Engineering Conference*, Stoke on Trent, United Kingdom, September 2015, pp. 1-6.

[2] Z. Qin, W. Li, and X. Xiong, "Incorporating multiple correlations among wind speeds, photovoltaic powers and bus loads in composite system reliability evaluation," *Applied Energy*, vol. 110, pp. 285-294, Oct. 2013.

[3] M. O. M. Mahmoud, M. Jaidane-Saidane, and N. Hizaoui, "The use of mixture of generalised Gaussian for trend analysis of the load duration curve: Summer and winter load variability in

Tunisia," in *Proc. 43rd International Universities Power Engineering Conference*, Padua, Italy, September 2008, pp. 1-5.
[4] L. Shi, S. Sun, L. Yao, Y. Ni, and M. Bazargan, "Effects of wind generation intermittency and volatility on power system transient stability," *IET Renewable Power Generation*, vol. 8, no. 5, pp. 509-521, 2013.
[5] Z. Q. Xie, T. Y. Ji, M. S. Li, and Q. H. Wu, "Quasi-Monte carlo based probabilistic optimal power flow considering the correlation of wind speeds using copula function," *IEEE Trans. on Power Systems*, vol. 33, no. 2, pp. 2239-2247, 2018.
[6] S. Ncwane and K. A. Folly, "Modeling wind speed using parametric and non-parametric distribution functions," *IEEE Access*, vol. 9, no. 1, pp. 104501-104512, 2021.
[7] Y. Li, Z. Yang, G. Li, D. Zhao, and W. Tian, "Optimal scheduling of an isolated microgrid with battery storage considering load and renewable generation uncertainties," *IEEE Trans. on Industrial Electronics*, vol. 66, no. 2, pp. 1565-1575, 2019.
[8] M. T. Hagh, P. Amiyan, S. Galvani, and N. Valizadeh, "Probabilistic load flow using the particle swarm optimisation clustering method," *IET Generation, Transmission & Distribution*, vol. 12, no. 3, pp. 780-789, 2018.
[9] H. Wang and B. Zou, "Probabilistic computational model for correlated wind speed, solar irradiation, and load using Bayesian network," *IEEE Access*, vol. 8, no. 1, pp. 51653-51663, 2020.
[10] J. Cai, Q. Xu, M. Cao, and B. Yang, "A novel importance sampling method of power system reliability assessment considering multi-state units and correlation between wind speed and load," *International Journal of Electrical Power Energy Systems*, vol. 109, pp. 217-226, Jul. 2019.
[11] R. Singh, B. C. Pal, and R. A. Jabr, "Statistical representation of distribution system loads using Gaussian mixture model," *IEEE Trans. on Power Systems*, vol. 25, no. 1, pp. 29-37, 2009.
[12] M. Nijhuis, M. Gibescu, and S. Cobben, "Gaussian mixture based probabilistic load flow for LV-network planning," *IEEE Trans. on Power Systems*, vol. 32, no. 4, pp. 2878-2886, 2017.
[13] P. Kundur, *Power System Stability and Control*, New York: McGraw-Hill, 1994.
[14] W. Asquith. (Accessed 10 April 2020). L-moments, censored L-moments, trimmed L-moments, L-comoments, and many distributions. [Online]. Available: https://cran.r-project.org/web/packages/lmomco/lmomco.pdf
[15] Q. Han, S. Ma, T. Wang, and F. Chu, "Kernel density estimation model for wind speed probability distribution with applicability to wind energy assessment in China," *Renewable and Sustainable Energy Reviews*, vol. 115, no. 1, pp. 1-14, 2019.
[16] B. Hu, Y. Li, H. Yang, and H. Wang, "Wind speed model based on kernel density estimation and its application in reliability assessment of generating systems," *Journal of Modern Power Systems and Clean Energy*, vol. 5, no. 2, pp. 220-227, 2017.
[17] J. Raz, E. J. Fernandez, and J. Gillespie, "Modeling NMR lineshapes using logspline density functions," *Journal of Magnetic Resonance*, vol. 127, no. 1997, pp. 173–183, 1997.
[18] M. Sahmoudi, K. Abed-Meraim, M. Lavielle, E. Kuhn, and P. Ciblat, "Blind source separation of noisy mixtures using a semi-parametric approach with application to heavy-tailed signals," in *Proc. 13th European Signal Processing Conference*, Antalya, Turkey, September 2005, pp. 1-4.
[19] F. Chen, H. Liu, J. Li, and X. Zhang, "Comparison of simulation methods of spatially correlated wind speeds," in *Proc. 5th International Conference on Electric Utility Deregulation and Restructuring and Power Technologies*, Changsha, China, November 2015, pp. 255-261.
[20] Y. Pan, L. Shi, and Y. Ni, "Modelling of multiple wind farms output correlation based on copula theory," *The Journal of Engineering*, vol. 2017, no. 13, pp. 2303-2308, 2017.
[21] Y. Zhang, S. Gao, J. Han, and M. Ban, "Wind speed prediction research considering wind speed ramp and residual distribution," *IEEE Access*, vol. 7, no. 1, pp. 131873-131887, 2019.
[22] University of Cyprus. IEEE 9-bus modified test system. [Online]. Available: https://www2.kios.ucy.ac.cy/testsystems/index.php/ieee-9-bus-modified-test-system/

Siyanda Ncwane received the B.Sc. degree in electrical engineering and M.Eng. degree in electrical engineering by coursework in 2009 and 2014, respectively, from the University of the Witwatersrand, Johannesburg, South Africa. He is currently pursuing an M.Sc. degree in electrical engineering with the University of Cape Town, Cape Town, South Africa. He currently works as a Chief Engineer in Strategic Grid Planning at the South African electricity utility Eskom. His research interests are in power system planning under high inverter-based generation and power system stability. Mr. Ncwane is registered with the Engineering Council of South Africa as a professional engineer and is also a member of the South African Institute of Electrical Engineers (SAIEE) and the IEEE.

Komla A. Folly received the BSc and MSc degrees in electrical engineering from Tsinghua University, Beijing, China, in 1989 and 1993, respectively. He received his Ph.D. degree in electrical engineering from Hiroshima University, Japan, in 1997. From 1997 to 2000, he worked at the Central Research Institute of Electric Power Industry (CRIEPI), Tokyo, Japan. He is currently a Professor in the Department of Electrical Engineering at the University of Cape Town, Cape Town, South Africa. In 2009, he received a Fulbright Scholarship and was a Fulbright Scholar at the Missouri University of Science and Technology, Missouri, USA. His research interests include power system stability, control and optimisation, HVDC modelling, grid integration of renewable energy, application of computational intelligence to power systems, smart grid, and power system resilience. He is a member of the Institute of Electrical Engineers of Japan (IEEJ), and a senior member of both the South African Institute of Electrical Engineers (SAIEE) and the IEEE.